Draft version November 24, 2016
Preprint typeset using LaTeX style AASTeX6 v. 1.0

arXiv:1611.07564v1 [astro-ph.HE] 21 Nov 2016

EVOLUTION OF HIGH-ENERGY PARTICLE DISTRIBUTION IN MATURE SHELL-TYPE SUPERNOVA REMNANTS

Houdun Zeng[1,3], Yuliang Xin[1,4], Siming Liu[1], J. R. Jokipii[5], Li Zhang[2,3], and Shuinai Zhang[1]

[1]Key Laboratory of Dark Matter and Space Astronomy, Purple Mountain Observatory, Chinese Academy of Sciences, Nanjing 210008, China, zhd@pmo.ac.cn; liusm@pmo.ac.cn

[2]Department of Astronomy, Yunnan University, Kunming, 650091, China

[3]Key Laboratory of Astroparticle Physics of Yunnan Province, Kunming, 650091, China

[4]University of Chinese Academy of Sciences, Yuquan Road 19, Beijing,100049, China

[5]University of Arizona, Tucson, Arizona, 85721, USA

ABSTRACT

Multi-wavelength observations of mature supernova remnants (SNRs), especially with recent advances in γ-ray astronomy, make it possible to constrain energy distribution of energetic particles within these remnants. In consideration of the SNR origin of Galactic cosmic rays and physics related to particle acceleration and radiative processes, we use a simple one-zone model to fit the nonthermal emission spectra of three shell-type SNRs located within 2 degrees on the sky: RX J1713.7−3946, CTB 37B, and CTB 37A. Although radio images of these three sources all show a shell (or half-shell) structure, their radio, X-ray, and γ-ray spectra are quite different, offering an ideal case to explore evolution of energetic particle distribution in SNRs. Our spectral fitting shows that 1) the particle distribution becomes harder with aging of these SNRs, implying a continuous acceleration process, and the particle distributions of CTB 37A and CTB 37B in the GeV range are harder than the hardest distribution that can be produced at a shock via the linear diffusive shock particle acceleration process, so spatial transport may play a role; 2) the energy loss timescale of electrons at the high-energy cutoff due to synchrotron radiation appears to be always a bit (within a factor of a few) shorter than the age of the corresponding remnant, which also requires continuous particle acceleration; 3) double power-law distributions are needed to fit the spectra of CTB 37B and CTB 37A, which may be attributed to shock interaction with molecular clouds.

Keywords: cosmic rays - gamma rays: ISM - ISM: supernova remnants - radiation mechanisms: non-thermal

1. INTRODUCTION

Supernova remnants (SNRs) have been considered as the dominant cosmic ray sources in the Galaxy since 1930s. Direct observational evidence for this paradigm comes from detection of radio and X-ray emission produced via the synchrotron process by GeV and TeV electrons, respectively, and γ-ray emission produced via three processes: inverse Compton (IC) scattering of low energy photons in the background and bremsstrahlung by relativistic electrons (leptonic processes), and decay of neutral pions produced in the inelastic hadronic interaction of high-energy ions with ambient nuclei (hadronic process)(Vink 2012). Determining the nature of the γ-ray emission plays an essential role in evaluating contributions of SNRs to the flux of Galactic cosmic rays observed near the Earth (Acero et al. 2016). Thanks to their excellent sensitivities, Cherenkov telescopes on the ground and the Large Area Telescope (LAT) on board the Fermi satellite have detected a few tens of supernova remnants with good spectral measurement in the γ-ray range during the past decade (Ferrand & Safi-Harb 2012; Carrigan et al. 2013; Acero et al. 2016), revealing a variety of γ-ray spectra (Yuan et al. 2012). Moreover analyses of *Fermi*-LAT and AGILE observations of SNRs W44, IC443 (Tavani et al. 2010; Giuliani et al. 2011; Ackermann et al. 2013), and W51C (Jogler & Funk 2016) have revealed tentative evidence for a low-energy spectral turnover associated with the π^0 decay process.

The SNR complex CTB 37, containing CTB 37A (G348.5+0.1), CTB 37B (G348.7+0.3) (and G348.5−0.0, which is not detected in the γ-ray range and will not be studied here), is an interesting region for comparative study of SNRs. The bright TeV SNR RX J1713.7−3946 (HESS J1713−397, also known as G347.3−0.5) locates within one

degree of this complex (Aharonian et al. 2006, 2008a). CTB 37A and 37B were discovered at radio wavelengths with very similar surface brightness ($\sim 8.5 \times 10^{-20}$ Wm^{-2}Hz^{-1}sr^{-1} at 20 cm), sizes ($\sim 10'$), and spectral indices ($\alpha \sim 0.3 - 0.5$) (Clark & Stephenson 1975; Kassim et al. 1991). At TeV energies, HESS J1713−381 and J1714−385 have been identified as the counterpart of CTB 37B and 37A, respectively (Aharonian et al. 2008a). All these three remnants have a central compact object and show a prominent shell (or half-shell) structure caused by shocks driven by core collapse supernovae. However, while the diffuse X-ray emission from RX J1713.7−3946 is dominated by synchrotron emission of TeV electrons (Katsuda et al. 2015), the diffuse X-ray emission from CTB 37A and CTB 37B are predominantly thermal. In the GeV range, RX J1713.7−3946 has a very hard spectrum, typical for young shell-type SNRs with prominent synchrotron X-ray emission (Acero et al. 2015). CTB 37A has a very soft spectrum (Brandt et al. 2013), typical for SNRs interacting with molecular clouds. The GeV spectrum of CTB 37B is a bit peculiar with a spectral peak near ~ 10 GeV (Xin et al. 2016). The above characteristics make these three SNRs to be ideal candidates for a comparative study of nonthermal emission from mature SNRs driven primarily by strong collisionless shocks to explore the evolution of energetic particle distribution in SNRs. Considering the SNR origin of Galactic cosmic rays, we propose a unified model with as few parameters as possible for the spectral fitting with the Markov Chain Monte Carlo (MCMC) algorithm (Lewis & Bridle 2002). The derived model parameters can be used to study the underlying physical processes of strong astrophysical shocks.

Our model is described in Section 2. In Section 3, we show results of the spectral fitting and compare them with previous studies. The conclusion and discussion are presented in Section 4.

2. MODEL DESCRIPTION

The physical processes of charged relativistic particle acceleration by inductive electric fields only depend on the particle rigidity $R = p/q$ explicitly, where p and q are the momentum and charge of the particle, respectively (Zhou et al. 2016). However the energy loss of high-energy electrons and ions via interactions with the background plasma are quite different. The radiative energy loss of electrons can make its energy distribution cutoff at an energy much lower than that for ions. We will assume that the distribution function of all particles has the following form

$$N(R_i) = N_{0,i} R_i^{-\alpha} \left(1 + \frac{R_i}{R_{\rm br}}\right)^{-1} \exp\left(\frac{-R_i}{R_{i,\rm cut}}\right) \Theta(R_i - R_{\rm min}) \quad (1)$$

where $R_i = p_i/q_i$ and 'i' represents different particle species, Θ is the Heaviside function, which is zero for negative argument and 1 for positive argument. For $R_{\rm min} < R_{\rm br} \ll R_{i,\rm cut}$, we have a double power-law distribution with an exponential high-rigidity cutoff. For $R_{\rm min} < R_{i,\rm cut} < R_{\rm br}$, the distribution function is approximately a single power-law with an exponential cutoff. Different particle species therefore have the same spectral break $R_{\rm br}$ and index α, but their high-rigidity cutoffs $R_{i,\rm cut}$ may be different. Motivated by the mechanism for formation of spectral breaks proposed by Malkov et al. (2011) and to simplify the model, we assume that for the broken power-law distribution, the spectral index increases by one toward higher rigidities. We set $R_{\rm min} = 1$ MeV$/ce$, where c and e are the speed of light and the elementary charge unit, respectively, so that electrons are still relativistic and can produce synchrotron emission efficiently. Considering the SNR origin of Galactic cosmic rays, we will assume that $K_{ep} = N_{0,e}/N_{0,p} = 0.01$ (Yuan et al. 2012) and the radiative effect of ions heavier than protons are included in $N_{0,p}$. The total energy content of protons above 1 GV$=1$ GeV$/ec$ then determines the normalization of the particle distributions.

With the relativistic particle distributions given above, the nonthermal radio to X-ray data can be fitted with the electron synchrotron processes (Ghisellini, Guilbert & Svensson 1988; Strong, Moskalenko & Reimer 2000) with the mean magnetic field B as a free parameter. For γ-ray emission, IC scattering of background soft photons by electrons (Jones 1968), electron bremsstrahlung (Strong, Moskalenko & Reimer 2000) and decay of neutral pions produced via proton-proton inelastic collisions are considered (Kamae et al. 2006). For the electron bremsstrahlung and hadronic processes, we assume that the background plasma has the same density. Then above ~ 100 MeV, the γ-ray flux produced via π^0 decay is always higher than that produced via the bremsstrahlung. For the IC scattering of electrons, besides the cosmic microwave background radiation (CMB), we include an infrared field with $T = 30$ K and an energy density of 1 eV cm^{-3} (Porter et al. 2006). The distance, source size, age, and the gas density in the emission region can be obtained from observations. The value of distance to an SNR is an extremely important quantity, which determines the size and energy contents in energetic particles and the magnetic field. Unfortunately, it is usually quite difficult to determine the distance precisely (Acero et al. 2016). These distances are often estimated as the kinematic distance of associated molecular clouds detected via CO lines (e.g. Castelletti et al. 2013), OH maser or HI absorption features (e.g. Tian & Leahy 2011, 2014). The extinction column density of optical and/or X-ray emission and/or the dispersion measure of the associated radio pulsar can also be use to constrain the distance (e.g. Arzoumanian et al.

2011). For shocks interacting with molecular clouds, given the complexity of this interaction process (Jones & Kang 1993; Inoue et al. 2012; Fukui et al. 2012; Sano et al. 2010, 2015), we will adjust the effective density for the emission process so that the total energy content in relativistic protons is on the order of 10^{50} erg, as required by the scenario of SNR origin of Galactic cosmic rays. Note that, since we are mainly interested in the overall emission spectrum, the effective density partly takes into account inhomogeneity of the ISM and uncertainties pertaining to interaction of cosmic rays with molecular clouds (Reach et al. 2005; Fukui et al. 2012; Sano et al. 2010, 2015).

Therefore, there are only 5 free parameters: α, $R_{\rm e,cut}$, $R_{\rm p,cut}$, $N_{0,\rm p}$, and the magnetic field for synchrotron emission B. Whenever necessary, a spectral break $R_{\rm br}$ is also introduced. Considering the radiative cooling effect of high-rigidity electrons, the synchrotron cooling timescale of electrons near $R_{e,cut}$,

$$\tau_{\rm syn} = 1.25\times10^3 \left(\frac{R}{1\rm TV}\right)^{-1} \left(\frac{B}{100\mu\rm G}\right)^{-2} \ \rm year\,, \tag{2}$$

should be longer than the diffusive shock acceleration timescale with Bohm diffusion (Lagage & Cesarsky 1983; Drury 1991),

$$\tau_{\rm acc} = 20\left(\frac{c^2R}{3BU^2}\right) = 20\left(\frac{R}{1\rm TV}\right)\left(\frac{B}{100\mu\rm G}\right)^{-1}\left(\frac{U}{10^3 km/s}\right)^{-2} \ \rm year\,, \tag{3}$$

where $1\rm TV = 1TeV/\mathit{ec}$. Then we have

$$R_{\rm e,cut} < 8\left(\frac{U}{10^3\rm km/s}\right)\left(\frac{B}{100\mu G}\right)^{-1/2} \ \rm TV\,, \tag{4}$$

where U is the shock speed. Note that for perpendicular shocks, the acceleration rate can be much higher, which will lead to a shorter acceleration timescale and a higher upper limit for the rigidity (Jokipii 1987). We will use the MCMC technique to constrain the model parameters. To find the best fit to observational data in a multi-dimensional model parameter space, the MCMC method is widely used for its high efficiency. In this approach, a Markov chain is built with the Metropolis-Hastings sampling algorithm that determines the jump probability from one point to another in the parameter space. For each parameter set $\mathbf{P}$, one obtains the likelihood function $L(\mathbf{P}) \propto \exp(-\chi^2(\mathbf{P})/\mathbf{2})$, where χ^2 is obtained by comparing model predictions with observations. A new set of parameter $\mathbf{P'}$ is adopted to replace the existing one $\mathbf{P}$ with a probability of $\min\{1, L(\mathbf{P'})/L(\mathbf{P})\}$. This sampling method ensures that the probability density distributions of model parameters are asymptotically approached with the number density of sampling points. The MCMC method has been reviewed by Liu et al. (2012) and described in detail by Neal (1993); Gamerman (1997); Lewis & Bridle (2002); Mackay (2003). Since this paper focuses on the overall emission spectra of SNRs, the magnetic field derived via the spectral fit should be interpreted as the spatially averaged value, similar to the effective density we adopted. Detailed studies of spatial structure of individual SNRs (e.g., Sano et al. 2015) are highly complementary to our results. For sources modeled with different effective densities, the Akaike information criterion, $\rm AIC = -2\ln\mathit{L}+2\mathit{k}$, where k is the number of model parameters (Liddle 2007), can be used to determine statistically which model is preferred by the data. The difference $\Delta = \rm AIC_2 - AIC_1 = \chi_2^2 - \chi_1^2 + 2k_2 - 2k_1$ determines the extent to which model 1 is favored over model 2. The relative probability that model 1 is statistically preferred is given by

$$P = \frac{\exp(-\rm AIC_1/2)}{\exp(-\rm AIC_1/2)+\exp(-\rm AIC_2/2)} = \frac{1}{1+\exp(-\Delta/2)}\,. \tag{5}$$

3. RESULTS

The left panel of Figure 1 shows the spectra and the best fit models for RX J1713.7−3946, CTB 37B, and CTB 37A. The corresponding model parameters are indicated by the dashed lines in the right panel. Table 1 gives the statistic-means and the corresponding errors for these parameters. Note that the best fit model parameters usually are slightly different from the statistic-means. Here for better comparing with previous studies, the rigidity parameters have been converted into the corresponding kinetic energy $E = [(Rqc)^2 + m^2c^4]^{1/2} - mc^2$, where m is the rest mass of the particle. The normalization of the proton distribution $N_{0,\rm p}$ has been converted into the total energy content of protons, W_p, above 1 GeV for a given density and distance. The total energy content in electrons with $E > 1$ GeV is indicated with W_e. W_B is the energy content in the magnetic field assuming a volume filling factor of unity, which should be considered as an upper limit since radio observations show that the magnetic field has filamentary structure and concentrates on a shell near the shock front (Reach et al. 2005).

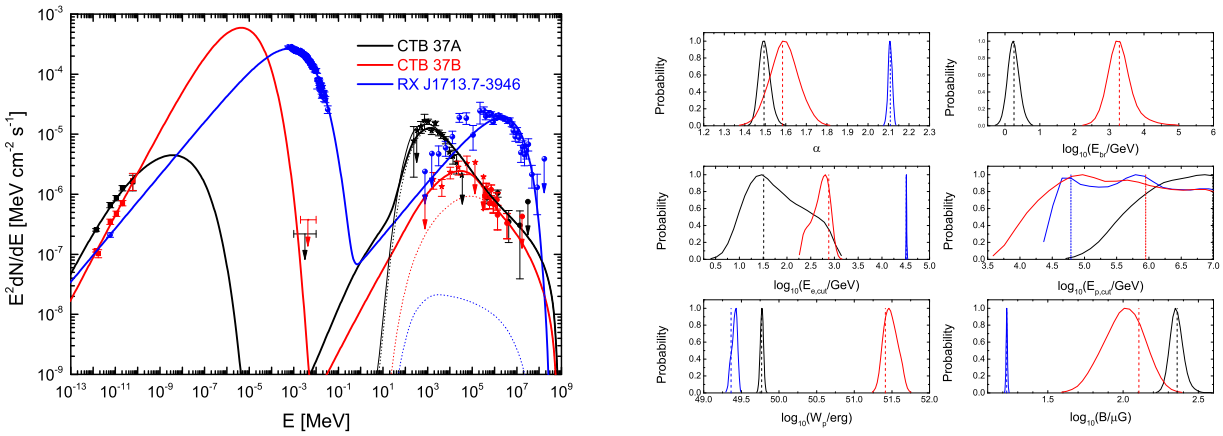

Figure 1. Left: The best fit model spectra for CTB 37A (Black line), CTB 37B (Red line), and RX J1713.7-3946 (Blue line). The corresponding model parameters are indicated by dashed lines in the right panel. For CTB 37B and RX J1713.7−3946, these spectra correspond to models with a gas density of n=0.5 cm^{-3} and n=0.01 cm^{-3}, respectively. The dotted lines show the hadronic component for these sources. The thin solid line for CTB 37A shows the γ-ray spectrum produced by protons with the high-energy power-law distribution extended to low energies without a spectral break. Right: 1-dimensional probability distribution of the model parameters. The vertical dashed lines indicate values for the best-fit model parameters.

3.1. *RX J1713.7−3946*

SNR RX J1713.7−3946 is a well-studied TeV bright shell-type SNR. Its emission spectrum is dominated by radiation of energetic particles. Only recently, very weak thermal X-ray emission has been detected from the inner region of the remnant (Katsuda et al. 2015). The spectra observed in radio, X-ray, GeV, and TeV bands, which are shown in Figure 1, are obtained from Acero et al. (2009); Tanaka et al. (2008); Federici et al. (2015), and Aharonian et al. (2011), respectively. The nature of its γ-ray emission is still being debated (Fukui et al. 2012; Federici et al. 2015). The dominance of the X-ray emission by energetic electrons via the synchrotron process and the hard GeV spectrum favors a leptonic model for the γ-emission (e.g., Yuan et al. 2012). The detection of molecular clouds and high density gas within/surrounding this remnant suggests that hadronic processes may also contribute to the γ-ray emission significantly (Sano et al. 2010, 2015; Inoue et al. 2012). Recent detailed studies (e.g. Sano et al. 2010, 2013, 2015; Fukui et al. 2012) show that RX J1713.7−3946 resides in an environment rich in molecular and atomic gases and there is a good spatial correspondence between TeV γ-ray and the interstellar gas, suggesting a hadronic origin for the γ-ray emission. However, assuming ionization equilibrium for the background plasma, Yuan et al. (2011) systematically investigated the parameter space of uniform one-zone emission models for the multi-wavelength emission of SNR RX J1713.7−3946, and concluded that the mean gas density should be less than 0.03 cm^{-3}, which is similar to the value of < 0.02 cm^{-3} derived from X-ray spectral analyses (Cassam-Chenaï et al. 2004). Given uncertainties in the shock cloud interaction and cosmic ray interaction with dense molecular clouds, we consider two effective values for the mean density of the emission region: 0.01 cm^{-3} and 1.0 cm^{-3}. An even higher value for the effective density will lead to prominent GeV emission via the hadronic process, therefore poor fit to the overall spectrum, and reduce the energy content in relativistic protons. Here, we also adopt a distance of 1 kpc, and a radius of ~ 10 pc for evaluation of the energy contents.

Given the high quality of the X-ray and γ-ray data and the relatively simple model proposed here, the model parameters are well-constrained and consistent with previous studies in the context of leptonic emission for the γ-rays (Fan et al. 2010; Yuan et al. 2011; Acero et al. 2015). For n=0.01 cm^{-3}, the magnetic field obtained by us (17.0 ± 0.2 μG) is slightly higher than that derived by Yuan et al. (2011) (12 μG). Such a differences may be attributed to the high energy density of 1 eV cm^{-1} adopted for the IR background photons and a 19% scaled down of the TeV fluxes (Aharonian et al. 2011). In any case, the obtained magnetic field is much lower than local values (of the order of mG) inferred from variability of X-ray filaments (Uchiyama et al. 2007; Inoue et al. 2012) and the value of $\sim 100\mu$G in the hadronic scenario for the γ-ray emission (Sano et al. 2015; Zirakashvili & Aharonian 2010). The synchrotron cooling time of 1340 years at $E_{e,\rm cut} = 32$ TeV, which is about 2 times lower than the upper limit given by equation (4) for a shock speed of 3000 km/s, is slightly lower the age of 1600 years commonly adopted in literature (Acero et al. 2009). A broken power-law model for electrons with synchrotron cooling time at the break energy equal to the age will not change other model parameters significantly. The high-energy cutoff of the proton distribution is not well constrained. A distinct spectral component above 100 TeV is expected if the high-energy cutoff exceeds

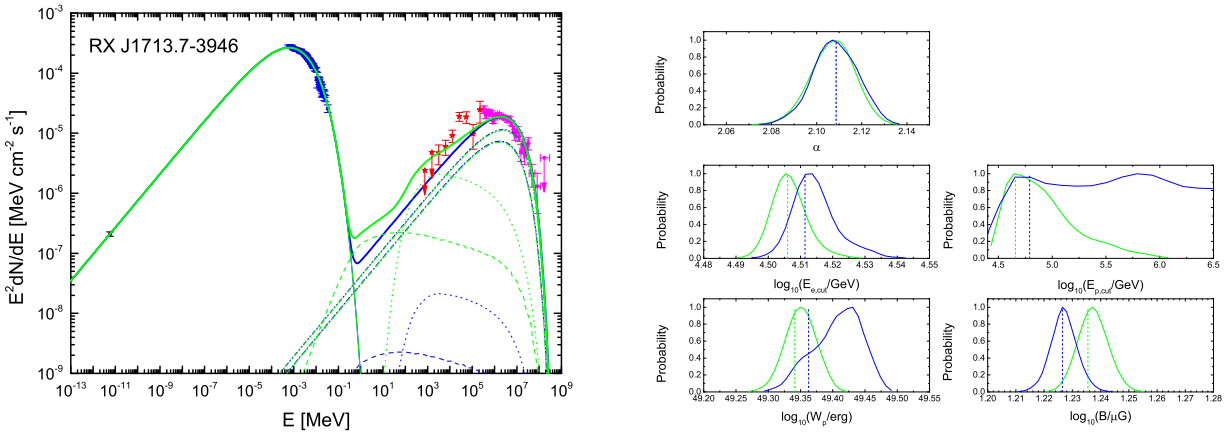

Figure 2. Left: Best fit spectra for RX J1713.7−3946 with two different values for the density of the background plasma. The blue lines are for the same model as shown in Figure 1. The green lines correspond to a model with a higher density (n= 1 cm^{-3}). The dashed lines are for the bremsstrahlung emission. The dashed-dotted lines and the dashed-dotted-dotted lines are for IC of the CMB and infrared photon fields, respectively. Right: 1-dimensional probability distribution of the model parameters. The vertical dashed lines indicate the best-fit values.

10^{15} eV, which can be tested with future observations. The total energy content of relativistic protons is 2.6×10^{49} erg, which is reasonable for a relatively young remnant, and the energy contents in electrons above 1 GeV and in the magnetic field are comparable as shown in earlier studies (Liu et al. 2008; Yang & Liu 2013). For n = 1.0 cm^{-3} (green lines in Figure 2 and the second row in Table 1 for RX J1713.7−3946), the model parameters have marginal changes except that the high-energy cutoff of the proton distribution can also be constrained to be 83 TeV.

Contributions to χ^2 from data in the radio, X-ray, GeV, and TeV bands for the two models are, respectively, 0.008, 380, 32.8, and 96.1 for $n = 0.01$ cm^{-3} and 0.07, 381, 20, and 81.2 for $n = 1.0$ cm^{-3}. The X-ray data dominate the value of χ^2 indicating that the one zone model with an exponential cutoff for the high-energy electron distribution may not give a sufficient description to the spatially integrated X-ray spectrum (Tanaka et al. 2008; Fan et al. 2010). Although compared with the model with $n = 0.01$ cm^{-3}, the improvement of the spectral model with $n = 1.0$ cm^{-3} is significant with a relative probability for the former of $\sim 10^{-6}$, the χ^2 in the GeV and TeV bands for $n = 1.0$ cm^{-3} are still quite high. Recently Abdalla et al. (2016) carried out detailed γ-ray spectral analysis of RX J1713.7−3946 and found that the combined GeV and TeV spectra favor a broken power-law distribution in both the leptonic and hadronic scenarios. Although the spectral fit may be improved significantly if we adopt a broken power-law distribution, the synchrotron cooling time at the break energy of a few TeV is at least 10 times longer than the age of the remnant (1600 yr). As pointed out by Abdalla et al. (2016), the temporal evolution of SNR may play a role in the formation of such a broken power-law spectrum, which should also improve the X-ray spectral fit (Ellison et al. 2012; Fan et al. 2013). Further exploration of this scenario will be presented in a separate paper.

Table 1. Spectral fitting parameters.

Source Name	α	$\log_{10}\frac{E_{\rm br}}{\rm GeV}$	$\log_{10}\frac{E_{\rm e,cut}}{\rm GeV}$	$\log_{10}\frac{E_{\rm p,cut}}{\rm GeV}$	$\frac{B}{\mu\rm G}$	$\log_{10}\frac{W_p}{\rm erg}$	$\frac{W_B}{W_e}$	Reduced χ^2 for the best-fit
RX J1713.7−3946	$2.11^{+0.01}_{-0.01}$	NA	$4.51^{+0.005}_{-0.006}$	> 4.51	$1.23^{+0.004}_{-0.004}$	$49.41^{+0.04}_{-0.04}+\log_{10}\left[\left(\frac{\rm n}{0.01\rm cm^{-3}}\right)^{-1}\left(\frac{\rm D}{1\rm kpc}\right)^2\right]$	$5.46\times\left(\frac{\rm D}{1\rm kpc}\right)^{-2}\left(\frac{\rm R}{10\rm pc}\right)^3$	$\frac{509}{240-5}=2.17$
RX J1713.7−3946	$2.11^{+0.01}_{-0.01}$	NA	$4.51^{+0.005}_{-0.005}$	$4.92^{+0.31}_{-0.31}$	$1.24^{+0.005}_{-0.005}$	$49.35^{+0.02}_{-0.02}+\log_{10}\left[\left(\frac{\rm n}{1.0\rm cm^{-3}}\right)^{-1}\left(\frac{\rm D}{1\rm kpc}\right)^2\right]$	$5.72\times\left(\frac{\rm D}{1\rm kpc}\right)^{-2}\left(\frac{\rm R}{10\rm pc}\right)^3$	$\frac{482}{240-5}=2.05$
CTB 37B	$1.59^{+0.07}_{-0.07}$	$3.31^{+0.29}_{-0.31}$	$2.70^{+0.18}_{-0.21}$	> 4.57	$2.00^{+0.13}_{-0.13}$	$51.49^{+0.10}_{-0.09}+\log_{10}\left[\left(\frac{\rm n}{0.5\rm cm^{-3}}\right)^{-1}\left(\frac{\rm D}{13.2\rm kpc}\right)^2\right]$	$32.9\times\left(\frac{\rm D}{13.2\rm kpc}\right)^{-2}\left(\frac{\rm R}{20\rm pc}\right)^3$	$\frac{13.7}{19-6}=1.05$
CTB 37B	$1.51^{+0.11}_{-0.11}$	$2.45^{+0.36}_{-0.34}$	$1.57^{+0.79}_{-0.78}$	> 4.60	$2.71^{+0.14}_{-0.15}$	$50.47^{+0.04}_{-0.04}+\log_{10}\left[\left(\frac{\rm n}{10.0\rm cm^{-3}}\right)^{-1}\left(\frac{\rm D}{13.2\rm kpc}\right)^2\right]$	$1.75\times10^4\times\left(\frac{\rm D}{13.2\rm kpc}\right)^{-2}\left(\frac{\rm R}{20\rm pc}\right)^3$	$\frac{14.3}{19-6}=1.10$
CTB 37A	$1.50^{+0.03}_{-0.03}$	$0.25^{+0.16}_{-0.16}$	$1.80^{+0.67}_{-0.61}$	> 6.18	$2.36^{+0.04}_{-0.04}$	$49.77^{+0.02}_{-0.02}+\log_{10}\left[\left(\frac{\rm n}{100\rm cm^{-3}}\right)^{-1}\left(\frac{\rm D}{7.9\rm kpc}\right)^2\right]$	$575\times\left(\frac{\rm D}{7.9\rm kpc}\right)^{-2}\left(\frac{\rm R}{10\rm pc}\right)^3$	$\frac{33.8}{21-6}=2.25$

NOTE—Errors are for 1σ statistical uncertainties; Lower limits correspond to 1σ confidence level; "NA" represents that the distribution is approximately a single power-law with an exponential cutoff.

3.2. *CTB 37A*

The radio data for CTB 37B and CTB 37A are taken from Kassim et al. (1991). SNR CTB 37A has a partial shell with an extended breakout to the south (Kassim et al. 1991). The distance to CTB 37A has been estimated from 21-cm absorption measurements to be 10.3 ± 3.5 kpc by Caswell et al. (1975). Recently, Maxted et al. (2013) and Tian & Leahy (2012) pointed out that CTB 37A and the $\sim 60 \mathrm{kms}^{-1}$ 1720 MHz OH masers in the direction should locate in the inner 3 kpc of the Galaxy, which implies a CTB 37A distance between 6.3 and 9.5 kpc. We will adopt a distance of 7.9 kpc in this paper.

CTB 37A does not have diffuse nonthermal X-ray emission. Using Chandra and XMM-Newton observations, Aharonian et al. (2008a) found diffusive thermal X-ray emission from the east part of the remnant and derived a flux upper limit of 3.5×10^{-13} erg cm^{-2}s^{-1} for nonthermal emission in the 1-10 keV range. Sezer et al. (2011) suggested that the diffuse thermal X-ray emission of CTB 37A is produced by shocked interstellar/circumstellar medium and estimated an ambient gas density of $\sim 1\ f^{-1/2}$ cm^{-3} and an age of $\sim 3 \times 10^4\ f^{1/2}$ yr, where f is the volume filling factor of the emitting plasma. Assuming a distance of 11.3 kpc, Pannuti et al. (2014) obtained similar results with an electron density $n_e = 0.77$ cm^{-3} and an age of $(3.2 - 4.2) \times 10^4$ yr by analyzing the X-ray spectrum. However the remnant is clearly interacting with molecular clouds. From velocity measurements of molecular clouds associated with the remnant, Reynoso & Mangum (2000) estimated the masses of individual clouds ranging from $1.3 \times 10^3\ M_\odot$ and $5.8 \times 10^4\ M_\odot$ with H_2 densities between 150 cm^{-3} and 660 cm^{-3} assuming a distance of 11.3 kpc, which implies a size of the remnant close to 28 pc. Based on the CS(1-0) emission, Maxted et al. (2013) obtained a density of $(3-10) \times 10^3$ cm^{-3} and a mass of $(500-2300) M_\odot$, which is consistent with the estimation given by Reynoso & Mangum (2000). We will assume an effective density of 100 cm^{-3} for calculation of the γ-ray emission and a radius of 10 pc for estimation of the energy content in the magnetic field.

HESS observations show that the TeV fluxes from CTB 37A and CTB 37B are comparable and CTB 37A has a slightly harder TeV spectrum than CTB 37B (Aharonian et al. 2008a). The GeV flux of CTB 37A is much higher than that of CTB 37B (Brandt et al. 2013). Using the Pass 8 data from the *Fermi*-LAT, we reanalysized the GeV spectrum of CTB 37A (Xin et al. 2016) and found that the GeV fluxes are systematically lower than those given by Brandt et al. (2013) due to identification of more sources nearby, and the overall γ-ray spectrum is consistent with a single power law model. However, compared with the radio spectrum of CTB 37B, the radio spectrum of CTB 37A shows clear evidence of softening toward high frequencies (Figure 1). We will adopt a broken power law model to fit the overall spectrum.

The inferred break energy is about 2 GeV (Table 1). Since the γ-ray emission is dominated by decay of π^0 for the high density adopted here, a broken power-law distribution with such a low break energy produces a γ-ray spectrum (black dotted line in Figure 1) almost identical to the γ-ray spectrum produced by protons with a single power-law distribution with a spectral index of 2.5 (thin black line in Figure 1). Therefore a broken power law distribution of high-energy protons is not necessary to reproduce the observed γ-ray spectrum. However, the radio spectrum justifying the broken power-law distribution. The synchrotron cooling time at the break (2 GeV) and the cutoff (63 GeV) energy of electrons are about 10^5 and 4000 years, respectively, which are compatible with the age ($\sim 3 \times 10^4$ years) of the hot plasma in the east part of the remnant. The fact that the synchrotron cooling time at the cutoff energy is more than 2 times shorter than the age of the remnant ($\sim 3 \times 10^4$ years) demands continuous electron acceleration in the late stage of the SNR evolution when the shock is interacting with molecular clouds.

We also infer a very hard distribution below 2 GeV, which is harder than even a strong shock produces at the shock front. This may be attributed to either compression of Galactic cosmic rays or Coulomb loss processes as suggested by Chevalier (1999) or to spatial transport processes away from the shock. The latter possibility will be discussed in a future publication (in preparation). We note that simple compression cannot change the power-law index. Also, the total energy content of protons with $E > 1$ GeV is about 10^{50} erg, which is consistent with the scenario of SNR origin for the Galactic cosmic rays, but more than 2 orders of magnitude higher than the energy content of Galactic cosmic rays within the shell of the remnant assuming an energy density of ~ 1 eV cm^{-3}. Simple compression of Galactic cosmic rays cannot reproduce the observed nonthermal emission.

A strong mean magnetic field of $\sim 230\ \mu$G is inferred, which can be attributed to shock interaction with molecular clouds. Indeed, strong magnetic fields ($0.2-1.5$ mG) in post-shock gas are estimated by Brogan et al. (2000) based on observations of OH (1720 MHz) masers from shocked molecular clouds. These fields are much higher than the value of 20 μG field inferred by Brandt et al. (2013) assuming a leptonic origin for the GeV emission. Such a strong magnetic field also leads to a higher energy content in the magnetic field than that in energetic electrons, as has been noticed in remnants slightly older than RX J1713.7−3946 (Yang et al. 2014). The energy contents in the magnetic field and

relativistic protons are actually comparable, which is consistent with the theoretical expectation for shock interaction with molecular clouds (Blandford & Cowie 1982).

Castro & Slane (2010) reported the detection of γ-ray emission of CTB 37A using data from *Fermi*-LAT, and found that the GeV spectrum can be fitted by a simple power-law model with a spectral index $\Gamma = -2.19 \pm 0.07$. They also found that a harder spectrum with an index of -1.46 ± 0.32 and a high-energy cutoff of 4.2 GeV gives a slightly improved fit to the *Fermi* data. Brandt et al. (2013) modeled the multi-wavelength spectrum of CTB 37A using a combination of leptonic and hadronic emission. The leptonic component has a power-law distribution with a spectral index of -1.75 and a high-energy cutoff of 50 GeV; the hadronic component has a power-law distribution with an index of -2.3. The GeV emission is dominated by the bremsstrahlung process while the TeV flux is dominated by hadronic emission. With the newly released *Fermi* data, we found that both the GeV and TeV emission can be attributed to energetic protons, and the model we have for the multi-wavelength spectrum is quite different from that proposed by Brandt et al. (2013). However, we notice that the value of reduced χ^2 of the best-fit model (2.25) is high with contributions to the χ^2 from the *Fermi* (22.7) and HESS (8.7) data dominant. Our best fit model has a γ-ray spectral index of -2.5, which is lower (softer) than that for the TeV spectrum and higher (harder) than that for the GeV spectrum. If future observations confirm γ-ray spectral hardening toward higher energies, which may be attributed to nonlinear diffusive shock acceleration (Ellison et al. 2012) or interaction of cosmic ray with molecular clouds (Gabici & Aharonian 2014), the simple spectral model proposed here will need to be revised to take into account the relevant physical processes.

3.3. *CTB 37B*

Since no prominent diffuse nonthermal X-ray emission is detected from CTB 37B, X-ray flux above 2 keV is treated as an upper limit for the nonthermal emission following Xin et al. (2016), who also gave the GeV data using the recently released Pass 8 data of the *Fermi*-LAT. It is interesting to note that the GeV spectrum appears to have a peak near 10 GeV. The spectrum of the diffuse thermal X-ray emission implies a low density of ~ 1 cm^{-3} and an age of ~ 5000 years (Aharonian et al. 2008b), which are consistent with a pre-shock electron density of 0.4 ± 0.1 cm^{-3} estimated by Nakamura et al. (2009) with a non-equilibrium collisional ionization model for Suzaku and Chandra observations. The distance to CTB 37B has been estimated to be 10.2 ± 3.5 kpc by Caswell et al. (1975), ≈ 8 kpc by Green et al. (2009) and a large value of ~ 13.2 kpc by Tian & Leahy (2012). We adopt the most recent distance estimate of 13.2 kpc in this paper.

Due to the absence of the synchrotron X-ray emission, Aharonian et al. (2008b) argued that the TeV emission should have a hadronic origin. A hadronic model will require a spectral break near a few hundreds of GeV to produce a γ-ray spectral peak near 10 GeV. Synchrotron X-ray emission is expected if the electron distribution extends into the TeV range. Therefore the electron distribution should be a single power law with a high-energy cutoff below 1 TeV while the proton distribution follows a broken power law with a spectral break at a few hundreds of GeV. With a background gas density of 0.5 cm^{-3}, Xin et al. (2016) found that the energy content of relativistic protons exceeds 10^{51} erg in the hadronic scenario. Even in the leptonic scenario for the γ-ray emission, they found that the energy content in electrons above 1 GeV is about one order of magnitude higher than that of other γ-ray remnants. Due to introduction of high-energy cutoffs below 10 TeV, their models produce TeV spectra much softer than the observed one. Adopting the same density for the background plasma, our best fit model results show a hybrid origin for the γ-ray emission with the hadronic and the IC process having comparable contribution in the GeV range (red lines in Figure 3). The TeV emission however is dominated by the hadronic process as suggested by Aharonian et al. (2008b). Due to contribution to the GeV emission via the IC process, the break energy of the proton distribution is about 20 TeV leading to a spectral peak near 100 GeV for the hadronic emission component (red dotted line in Figure 1). The model also produces a TeV spectrum slightly softer than that for CTB 37A, which is consistent with HESS observations (Aharonian et al. 2008a).

We infer a strong magnetic field of 100 μG and a very high energy content of $\sim 3 \times 10^{51}$ erg in relativistic protons, which are consistent with the results of Xin et al. (2016). The energy content in the magnetic field is slightly higher than that in GeV electrons compatible with the evolution of younger remnants (Yang et al. 2014; Guo et al. 2012). The high-energy cutoff of the electron distribution is about 500 GeV which is mostly constrained by the observed GeV emission via the IC process. The synchrotron cooling time at the cutoff energy of electrons is about 2800 years, which is about two times shorter than the age estimate (~ 5000 years). Taking into account the effect of synchrotron loss on the electron distribution, one may adopt a broken power-law distribution for electrons with a break energy below 200 GeV for the magnetic field inferred above. Such a model may reproduce the observed spectrum if one includes optical photons in the background, which may contribute to the GeV γ-ray emission significantly. We will not explore this

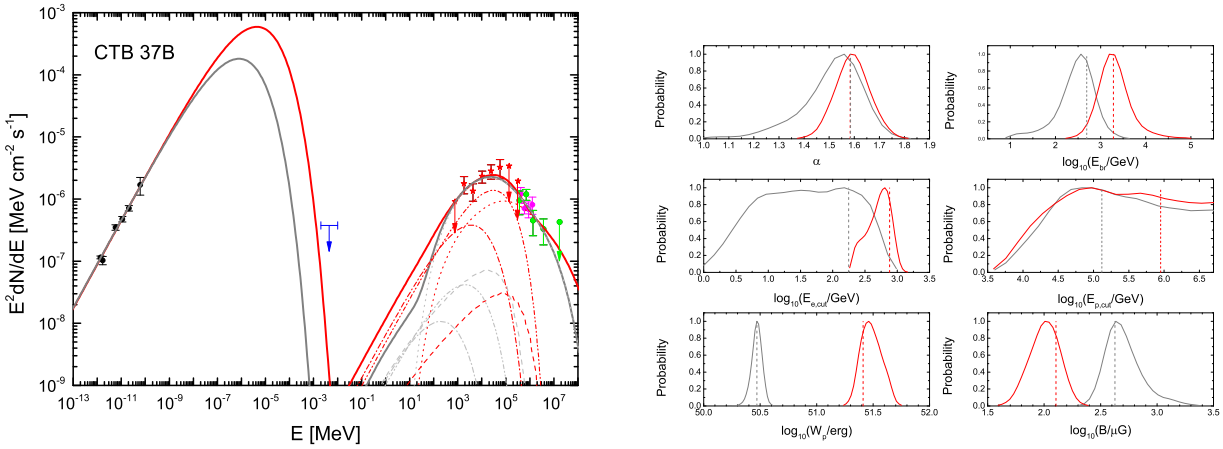

Figure 3. Left: Best fit spectra for CTB 37B with two different values for the density of the background plasma. The red lines are for the same model shown in Figure 1. The gray lines correspond to a model with a higher density of n=10 cm^{-3}. The dashed lines are for the bremsstrahlung emission. The dash-dotted lines and the dash-dotted-dotted lines are for IC of the CMB and infrared photon fields, respectively. Right: 1-dimensional probability distribution of the model parameters. The vertical dashed lines indicate the best-fit values.

model in details since the model parameters will not change dramatically.

We also infer a very hard distribution with an index of 1.6 from hundreds of MeV to hundreds of GeV for electrons and to tens of TeV for protons. Such a distribution cannot be attributed to compression of Galactic cosmic rays or Coulomb loss processes. Nonlinear diffusive shock acceleration will not produce a single power-law distribution with a very hard spectrum. Stochastic particle acceleration by compressible turbulence in the downstream of the shock may be able to account for such a hard spectrum (Ostrowski 1999; Bykov et al. 2000; Liu et al. 2008; Fan et al. 2013). As mentioned above, spatial transport of accelerated particles away from the shock front will also produce a harder spectrum.

We notice that there is increasing evidence that CTB 37B may be interacting with molecular clouds (Frail et al. 1996; Tian & Leahy 2012; Jiang et al. 2015). The broken power-law distribution of relativistic protons also favors shock interaction with molecular clouds. By adopting an effective density of 10 cm^{-3}, the γ-ray emission is then dominated by the hadronic process and the energy content of relativistic protons is reduced by more than one order of magnitude, which is comparable to other γ-ray remnants (See gray lines in Figure 3 and the second row in Table 1 for CTB 37B). The break energy is reduced to about 300 GeV in this case leading to a γ-ray spectral peak near 10 GeV. However, a stronger magnetic field of 0.5 mG is needed to reproduce the radio fluxes for the decrease of $N_{0,e}$, which also suppresses contributions to γ-rays by the IC process. For a volume filling factor of a few percent, which is compatible with radio observations, the energy content of the magnetic field will be comparable to that of relativistic protons. The synchrotron cooling time of electrons at the cutoff energy of 40 GeV is about 1900 years, which is about 2 times shorter than the age estimate ($\sim$ 5000 years), implying continuous particle acceleration.

A harder distribution with an index of 1.51 is inferred due to the decrease of the cutoff energy for the electron distribution. Such a distribution also challenges the diffusive shock particle acceleration theory and may imply continuous particle acceleration downstream of the shock (Bykov et al. 2000; Liu et al. 2008; Malkov et al. 2011). Spatial transport from the shock may also harden the spectrum (Jokipii and Liu, in preparation). In W44, Uchiyama et al. (2010) shows that the hard radio spectrum may be attributed to secondary electrons and positrons produced in the pp elastic collisions. The radio emission of CTB 37B cannot be attributed to secondary electrons and positrons since the radio luminosity is comparable to the γ-ray luminosity. Compared with the model (red lines in Figure 3) with a lower effective density of 0.5 cm^{-3}, this model (grey lines in Figure 3) with an effective density of 10 cm^{-3} reduces the overall energy content to a value of $\sim 10^{50}$ erg compatible with typical SNRs and in agreement with the SNR origin of Galactic cosmic ray. A reduced χ^2 of $\sim$ 1 shows that both models give equally good fit to the broadband spectra. An even higher value for the effective density will lead to a stronger magnetic field and less energy content in relativistic protons, which requires a smaller volume filling factor for the magnetic field and relativistic protons to maintain energy equipartition (Blandford & Cowie 1982). More observations are needed to confirm shock interaction with molecular clouds in this remnant (Jiang et al. 2015).

Recently, Xin et al. (2016) reported the gamma-ray emission of CTB 37B by using 7-year *Fermi*-LAT data, and found that the multi-wavelength spectrum can be well fitted with a leptonic or a hadronic model. The parameters of

their leptonic model are similar to ours except for a slightly higher cutoff energy of the electron distribution for the absence of hadronic contribution to the γ-rays, which also leads to a deficit in the model predicted TeV flux. In their hadronic model, electrons and protons have softer distributions with different spectral indexes. The proton distribution cuts off at 3 TeV with an energy content much higher than ours for the adoption of a lower density of the background plasma, which leads to a value of K_{ep} more than one order of magnitude lower than ours. Our magnetic field of 0.5 mG is more than 2 times higher than their value for the lower energy content of electrons in our model. In order to estimate the diffuse neutrino flux from SNRs, Mandelartz & Tjus (2015) use a similar one-zone model to perform multi-wavelength spectral fit to 22 SNRs. CTB 37A and CTB 37B are among those sources. However, they adopted a single power-law distribution and the normalization, spectral index, and cutoff energy of the electron distribution are independent of those for protons. Their model parameters in general are not as well constrained as ours and, with the recently released *Fermi* data, we have an up-to-date GeV flux measurement for both sources.

4. CONCLUSION AND DISCUSSION

Considering the SNR origin of Galactic cosmic rays and physical processes related to acceleration and radiation of high-energy particles, we propose a simple one-zone emission model with at most 6 parameters for nonthermal emission spectrum of shell type SNRs driven by shocks of supernova explosions. The model assumes that the ratio of the normalization of electron distribution to that of protons is 0.01 and adopts reasonable values for the effective density of background plasma in the emission region. With the MCMC algorithm, multi-wavelength spectral measurement of SNRs can be used to constrain other parameters related to radiation of relativistic particles in these remnants. Using three shell type SNRs located within 2 degrees on the sky and having distinct γ-ray spectra as examples, we carried out detailed spectral fitting and studied the physical implications of the model parameters.

By fitting SNRs with distinct γ-ray spectra with a unified model, it is possible to explore evolution of energetic particle distributions in SNRs. We find that in general the particle distribution becomes harder with aging of the shock and it is challenging to explain the hard electron distribution in CTB 37B via the diffusive shock particle acceleration, compression of Galactic cosmic rays, secondaries of the pp process, and/or via Coulomb loss processes. Continuous particle acceleration in the shock downstream by compressible turbulence may produce a very hard distribution (Liu et al. 2008). We also suggest that spatial transport of cosmic rays away from the shock may account for the hard observed spectrum. The synchrotron energy loss time at the high-energy cutoff of the electron distribution is always shorter than and appears to increase with the age of the corresponding remnant, which also requires continuous acceleration and suggests that a time-dependent approach may be necessary to study the bulk of the particle acceleration in SNRs as is the case for a stochastic particle acceleration model proposed by Fan et al. (2013). These results suggest that, for mature SNRs, the classical diffusive shock acceleration process may not dominate the overall particle acceleration. Detailed studies of spatial structure of individual SNRs may be used to separate features associated with shock acceleration from other nonthermal features to determine the dominant particle acceleration processes (Sano et al. 2015; Abdalla et al. 2016).

Our model predicts a correlation between the radio and γ-ray spectral hardness, which naturally produces a TeV spectrum in CTB 37A harder than that in CTB 37B. However given the complexity of processes involved in the formation of electron distribution in the GeV range and the three γ-ray emission processes, such a correlation may not be evident in the observed data and detailed spectral fit is needed. By adjusting the effective density of ions in the background plasma for relativistic proton interaction with, the overall energy content in relativistic protons can be confined on the order of 10^{50} erg, which agrees with the SNR origin of Galactic cosmic rays. Other model parameters derived with such a constraint are also compatible with measured characteristics of these SNRs.

For the sake of simplicity, we do not consider the temporal and spatial evolution of SNR, the radiative cooling effect on the distribution of high-energy electrons, the effects of Galactic cosmic ray compression by shocks and Coulomb collisional energy loss on the distribution of relatively low-energy electrons. We also assume that the spectral index increases by one from low to high energies for the broken power-law distribution. For the three SNRs studied here, these simplifications do not seem to affect the main conclusions above. However the relatively high values of the reduced χ^2 for CTB 37A and RX J1713.7−3946 suggest that revision of this simple model is necessary to improve the spectral fit. *Fermi* γ-ray observations have revealed a variety of spectral shape (Ackermann et al. 2013; Acero et al. 2016). Over the past few years, similar models have been applied to study of individual SNRs. The model parameters for W51 derived by Aleksić et al. (2012) are very similar to those for CTB 37A. The γ-ray spectrum of young SNR G349.7+0.2 (Abramowski et al. 2015) has a spectral break above 10 GeV, reminiscence of the γ-ray spectrum of CTB 37B. Application of a uniform model to these SNRs is essential to probe the evolution of energetic particle distribution in SNRs. It will also guide further development of the model to incorporate more physical processes affecting the

evolution of energetic particle distribution in SNRs.

We would like to thank the anonymous referee for very helpful comments, which help to improve the paper significantly. This work is partially supported by the Strategic Priority Research Program, the Emergence of Cosmological Structures, of the Chinese Academy of Sciences, Grant No. XDB09000000, the Key Laboratory of Particle Astrophysics of Yunnan Province (Grant 2015DG035), and the NSFC grants 11173064, 11233001, and 11233008. LZ acknowledges partial funding support by the National Natural Science Foundation of China (NSFC) under grant No. 11433004.

REFERENCES

Abdalla, H., et al. (HESS Collaboration) 2016 (ArXiv:1501,06054)
Abramowski, A., et al. (HESS Collaboration) 2015, A&A, 574, A100
Acero, F., et al. 2009, A&A, 505, 157
Acero, F., Lemoine-Goumard, M., Renaud, M., Ballet, J., Hewitt, J. W., Rousseau, R., & Tanaka, R. 2015, A&A, 580, A74
Acero, F, et al. 2016, ApJS 224, 8
Ackermann, M., Ajello, M., Allafort, A., et al. 2013, Science, 339, 807
Aharonian, F., et al. (HESS Collaboration) 2006, ApJ, 636, 777
Aharonian, F., et al. (HESS Collaboration) 2008a, A&A, 490, 685
Aharonian, F., et al. (HESS Collaboration) 2008b, A&A, 486, 829
Aharonian, F., et al. (HESS Collaboration) 2011, A&A, 531, C1
Aleksić, J., et al., 2012, A&A, 541, A13
Arzoumanian, Z., Gotthelf, E. V., Ransom, S. M., et al. 2011, ApJ, 739, 39
Blandford, R. D., & Cowie, J. J. 1982, ApJ, 260, 625
Brandt T J., (Fermi-LAT Collab.), 2013, J. Adv. Space Res., 51, 247
Brogan C., Frail D., Goss W. & Troland T., 2000, ApJ, 537, 875-890
Bykov, A. M., Chevalier, R. A., Ellison, D. C., & Uvarov, Yu. A. 2000, ApJ, 538, 203
Carrigan, S., Brun, F., Chaves, R. C. G., et al. 2013, ICRC, arXiv:1307.4690
Castelletti, G., Supan, L., Dubner, G., Joshi, B. C., & Surnis, M. P. 2013, A&A, 557, L15
Castro, D. & Slane, P., 2010, ApJ, 717, 372-378
Caswell, J. L., Murray, J. D., Roger, R. S., Cole, D. J., & Cooke, D. J. 1975, A&A, 45, 239
Cassam-Chenaï, G., Decourchelle, A., Ballet, J., Sauvageot, J. L., Dubner, G., & Giacani, E. 2004, A&A, 427, 199
Chevalier, R. A. 1999, ApJ, 511, 798
Clark, D. H., & Stephenson, F. R. 1975, The Observatory, 95, 190
Drury, L. O'C. 1991, MNRAS, 251, 340
Ellison, D. C., Slane, P., Parnaude, D. J., &Bykov, A. M. 2012, ApJ, 744:39
Fan, Z. H., Liu, S. M., Yuan, Q., & Fletcher, L. 2010, A&A, 517, L4
Fan, Z. H., & Liu, S. M. 2013, Proceeding of the 3rd Galileo-Xu Guangqi Meeting, 23, 319
Federici, S., Phol, M., Telezhinsky, I., Wilhelm, A., & Dwarkadas, V. V., 2015, A&A, 577, A12
Ferrand, G., & Safi-Harb, S. 2012, Advances in Space Research, 49, 1313-1319
Fukui, Y.; Sano, H.; Sato, J. et al. 2012, ApJ, 746, 82
Frail, D. A., et al., 1996, AJ, 111,1651
Gamerman, D. 1997, Markov Chain Monte Carlo: Stochastic Simulation for Bayesian Inference (Chapman and Hall, London)
Ghisellini, G., Guilbert,P. W. & Svensson, R., 1988, 334, L5
Giuliani, A. et al., 2011, ApJL, 742, L30
Gabici, S., & Aharonian, F. A. 2014, MNRAS, 445, L70
Green, D. A. 2009, Bull. Astron. Soc. India, 37, 45
Guo, F., Li, S. T., Li, H., Giacalone, J., Jokipii, J. R., & Li, D. 2012, ApJ, 747, 98
Inoue, T., Yamazaki, R., Inutsuka, S., Fukui, Y. 2012, ApJ, 744, 71
Jiang, B. et al. 2015, IAU, Meeting #29, id.2255641
Jogler, T., & Funk, S. 2016, ApJ, 816, 100
Jokipii, J. R. 1987, ApJ, 313, 842
Jones, T. W., & Kang, H. S. 1993, ApJ, 402, 560
Jones, F. C. 1968, Physical Review, 167, 1159
Kamae, T., Karlsson, N., et al. 2006, 647, 692
Kassim, N. E., Weiler, K. W., & Baum, S. A. 1991, ApJ, 374, 212
Katsuda, S., et al. 2015, ApJ, 814, 29
Lagage, P. O., & Cesarsky, C. J. 1983, A&A, 125,249
Lewis, A., & Bridle, S. 2002, Phys. Rev. D, 66, 103511
Liddle, A. R. 2007, MNRAS, 377, L74
Liu, S. et al., 2008, ApJL, 683, L163
Liu, J., Yuan, Q., Bi, X. J., Li, H., & Zhang, X. M. 2012, Phys. Rev. D, 85, d3507
Mandelartz, M. & Tjus, J. B., 2015, Astroparticle Physics, 65, 80
Mackay, D. J. C. 2003, Information Theory, Inference and Learning Algorithms (Cambridge University Press)
Malkov, M. A., Diamond, P. H., & Sagdeev, R. Z. 2011, Nature, DOI:10.1038/ncomms1195
Maxted, N. I., Rowell, G. P. et al. 2013, MNRAS, 434, 2188
Nakamura, R. et al. 2009, PASJ, 61, S197
Neal, R. M. 1993, Probabilistic Inference Using Markov Chain Monte Carlo Methods (Department of Computer Science, University of Toronto)
Ostrowski, M. 1999, A&A, 345, 256
Pannuti, T. G., Rho, J., Heinke, C. O., Moffitt, W. P., 2014, AJ, 147, 55
Porter, T. A., Moskalenko, I. V., & Strong, A. W., 2006, ApJ, 648, L29
Reach, W. T., Rho, J., & Jarrett, T. H., 2005, ApJ, 618, 297
Reynoso, E. M., & Mangum, J. G., 2000, ApJ, 545, 874
Sano, H., Sato, J., Horachi, H., et al. 2010, ApJ, 724, 59
Sano, H., Tanaka, T., Torii, K., et al. 2013, ApJ, 778, 59
Sano, H., Tanaka, T., Torii, K., et al. 2015, ApJ, 799, 175
Sezer A., Gok F., HudaverdiM. & Ercan E., 2011, MNRAS, 417, 1387-1391
Strong, A. W., Moskalenko, I. V. & Reimer, O., ApJ, 2000, 537, 763.
Tanaka, T., et al. 2008, ApJ, 685, 988
Tavani, M., et al., 2010, ApJL, 710, L151
Tian, W. W., & Leahy, D. A. 2011, ApJ, 729, L15
Tian, W. W., & Leahy, D. A. 2012, MNRAS, 421, 2593
Tian, W. W., & Leahy, D. A. 2014, ApJ, 783, L2
Uchiyama, Y., et al., 2007, Nature, 449, 576
Uchiyama, Y., et al., 2010, ApJL, 723, L122
Vink, J. 2012, Astron. Astrophys. Rev, 20, 49

Xin, Y. L., Liang, Y. F., Li, X., Yuan, Q., Liu, S. M., Wei, D. M., 2016, ApJ, 871, 64
Yang, C. Y., & Liu, S. M. 2013, ApJ, 773, 138
Yang, R. Z., Zhang, X., Yuan, Q., & Liu, S. M. 2014, A&A, 567, A23
Yuan, Q., Liu, S. M.,Fan, Z. H., Bi, X. J., & Fryer, C. L. 2011, ApJ, 735, 120
Yuan, Q., Liu, S. M., & Bi, X. J. 2012, ApJ, 761, 133
Zhou, X., Büchner, J., Bárta, M., Gan, W., Liu, S. 2016, ApJ, 827, 94
Zirakashvili, V. N., & Aharonian, F. A. 2010, ApJ, 708, 965